Journal of Renewable and Sustainable Energy ARTICLE scitation.org/journal/rse

Multi-timescale operations of nuclear-renewable hybrid energy systems for reserve and thermal product provision

Cite as: J. Renewable Sustainable Energy **15**, 025901 (2023); doi: 10.1063/5.0138648
Submitted: 13 December 2022 · Accepted: 12 February 2023 ·
Published Online: 8 March 2023

View Online Export Citation CrossMark

Jubeyer Rahman and Jie Zhang[a)]

AFFILIATIONS

The University of Texas at Dallas, Richardson, Texas 75080, USA

Note: This paper is part of the special issue on Hybrid Renewable Energy Systems.
[a)]**Author to whom correspondence should be addressed:** jiezhang@utdallas.edu

ABSTRACT

In this paper, an optimal operation strategy of a nuclear-renewable hybrid energy system (N-R HES), in conjunction with a district heating network, is developed within a comprehensive multi-timescale electricity market framework. The grid-connected N-R HES is simulated to explore the capabilities and benefits of N-R HES of providing energy products, different reserve products, and thermal products. An N-R HES optimization and control strategy is formulated to exploit the benefits from the hybrid energy system in terms of both energy and ancillary services. A case study is performed on the customized NREL-118 bus test system with high renewable penetrations, based on a multi-timescale (i.e., three-cycle) production cost model. Both day-ahead and real-time market clearing prices are determined from the market model simulation. The results show that the N-R HES can contribute to the reserve requirements and also meet the thermal load, thereby increasing the economic efficiency of N-R HES (with increased revenue ranging from 1.55% to 35.25% at certain cases) compared to the baseline case where reserve and thermal power exports are not optimized.

NOMENCLATURE

Sets

B	Set of all buses
B_L	Set of load buses
B_{HES}	Set of HES buses
G	Set of generators
G_{HES}	Set of HES generators
G_{REN}	Set of renewable generators
J	Set of DHN junctions
L	Set of transmission lines
RS	Set of reserve types
T	Set of time slots

Parameters

C_g^k	Generation cost of unit g in block k
$D_{b,t}$	Load at bus b at the tth interval
$D_{\text{thermal},t}$	Thermal load at the tth interval
DD	Duration of the shut-down process
DT_g	Minimum down time of unit g
H_{DAC}	Number of intervals for DASCUC
H_{RTC}	Number of intervals for RTSCUC
H_{RTD}	Number of intervals for RTSCED
I_{DAC}	Interval length for DAC
I_{RTC}	Interval length for RTC
I_{RTD}	Interval length for RTD
IDT_g	Initial minimum down time of unit g
$IF_{b,g}$	Injection factor of unit g at bus b
ISA_g	Number of intervals before startup of unit g
IUT_g	Initial minimum up time of unit g
K_g	Number of blocks in generation cost function of unit g
Limit_l	Power flow limit at line l
NL_g	No-load cost of unit g
$P_{g,t}^{\text{forecast}}$	Renewable power forecast of unit g at the tth interval
$P_g^{\max}$	Maximum output of unit g
$P_g^{\min}$	Minimum output of unit g
$PSCS_g$	Whether the unit g retained its "on" status before the horizon
$PTDF_{l,b}$	Power transfer distribution factor from bus b to line l
R_g^D	Ramp-down limit for unit g

R_g^U	Ramp-up limit for unit g
R_g^{SD}	Ramp-down limit for unit g at shutdown
R_g^{SU}	Ramp-up limit for unit g at startup
$RC_{g,r}$	Reserve cost of unit g for type r
$RP_{t,r}$	Reserve price at the tth interval for type r
$RRR_{t,r}$	System reserve requirement of type r at time t
SD_g	Shut-down cost of unit g
SU_g	Start-up cost of unit g
TDP_g	Shut-down period of unit g
TUP_g	Start-up period of unit g
UD	Duration of the start-up process
UT_g	Minimum up time of unit g
$VOIR_r$	Cost of insufficient reserve of type r
ΔP_g^k	Generation block size of unit g in block k
η	Electrical to thermal power conversion factor

Variables

$\delta_{b,t}$	Load shedding quantity of bus b at the tth interval
$\bar{p}_{g,t}$	Maximum available power output of unit g at the tth interval
$p_{g,i}^D$	Power output of unit g at the tth interval during interval shutdown
$p_{g,i}^U$	Power output of unit g at the tth interval during interval startup
$\Theta_{j,t}$	Temperature at j junction at the tth interval
$ir_{t,r}$	System level insufficient reserve quantity of type interval r at the tth interval
$lf_{l,t}$	Line flow at line l at the tth interval
$ll_{thermal,t}$	Loss of thermal load at the tth interval
ls_t	Load-shedding penalty at the tth interval
$\text{net}_{t,r}^{rr}$	Net reserve export of type r from HES at interval the tth interval
net_t^p	Net power export from HES at the tth interval
$p^{b,g,t}$	Power output of unit g at bus b at the tth interval
$p_{g,t}$	Power output of unit g at the tth interval
$pc_{g,t}$	Production cost of unit g at the tth interval
$p_{g,t}^k$	Power output of unit g at the tth interval in block k
$p_{b,t}^{net}$	Net power injection at bus b at the tth interval
$P_{j,t}$	Pressure at j junction at the tth interval
Q_t	Thermal dispatch from HES at the tth interval
$rc_{g,t,r}$	Reserve cost of unit g of type r at the tth interval
$rr_{g,t,reg}$	Regulating reserve from unit g at the tth interval
$rr_{g,t,r}$	Reserve of type r from unit g at the tth interval
$sd_{g,t}$	Shut-down cost of unit g at the tth interval
$su_{g,t}$	Start-up cost of unit g at the tth interval
$v_{g,t}$	Commitment status of unit g at the tth interval
$y_{g,t}$	Starting-up status of unit g at the beginning of the interval tth interval
$z_{g,t}$	Shutting-down status of unit g at the beginning of the interval tth interval

I. INTRODUCTION

Flexibility requirement has seen a drastic rise in power systems in recent years to accommodate the growing renewable generation fleet.[1] Research efforts have been targeted to harness flexibility through utilizing existing resources (e.g., energy storage, flexible generation, etc.), introducing new operational strategies (e.g., demand response, sector coupling, and flex-ramp reserve[2]), deploying improved renewable forecasts,[3] and exploring new technologies (e.g., high-voltage direct current[4,5]). The coupling between different sectors has gained increasing attention due to additional tradable energy products besides providing flexible headroom to system operators.[6] Generally, the sector coupling is made at a suitable load center convenient for dispatching energy products through different energy networks, rather than distributing it all over the energy system, thus making the success of coupled operation rely on a single point of common coupling. This poses the system in a position of potential vulnerable exposures to contingency events.[7] Since the distributed placement of sector-coupled systems may not be available in the near future due to technical and budgetary constraints, alternative solutions ensuring the reliable operation of the coupled system are desired. One of the possible solutions could be self-sufficient hybrid energy systems (HES) or more broadly integrated energy systems.[8]

The advent of more flexible small modular reactors (SMRs) and the proved synergy between nuclear and renewable resources make SMRs a promising component for HES,[9] due to their almost zero carbon footprint and small operational costs.[10–12] SMRs could be coupled together with renewable generators to form a nuclear-renewable hybrid energy system (N-R HES). Thermal or gas systems could also be incorporated to further enhance the flexibility of the system to leverage virtual storage.[13] Sector coupled N-R HES offers a suite of services at different timescales to promote a more secure and reliable integration of renewable energy into the system,[14] such as ancillary services. Ancillary services are typically used by grid operators to reduce imbalances due to uncertainties brought by variable load and renewable energy resources and to protect the system against contingency events. N-R HES could provide a range of ancillary services at multiple timescales, such as flexible ramping reserves, regulation reserves, and frequency response, to reduce the operational risk and enhance the reliability of the system.[15,16]

Three types of N-R HES have been studied in the literature:[17] tightly coupled, thermally coupled, and loosely coupled N-R HES. Tightly coupled N-R HESs are co-located, directly integrated, and co-controlled behind the grid. Thermally coupled N-R HESs have an integrated thermal connection and are co-controlled, but may have multiple electrical connections to the grid and subsystems may not be co-located. Loosely coupled (or electricity-only) N-R HESs only have electrical interfaces and subsystems that can be located separately with multiple connections to the grid, but they are co-controlled, so a single management entity dispatches the energy and services to the grid. This work focuses on optimizing the operation of a tightly coupled N-R HES, to extract flexibility in terms of various reserve products.

The conventional role of nuclear plants as base-load serving units has recently been transformed into (i) managing the volatility of the growing renewable generation and (ii) reaping additional benefits by providing different energy and power products. In some countries, such as France and Germany, system operators have already started to use nuclear plants in load-following regulation services.[18] Studies[19] have shown potential benefits and versatility of N-R HES integration to the power grid, while earning additional revenues through participating into the ancillary service market besides the energy market.

Though N-R HES is preferable over their standalone counterparts,[20] its interaction with the rest of the grid in different market settings remains mostly unexplored. A previous study[21] has explored the impact of N-R HES on forward (day-ahead) market and spot (real-time) market in a price taker role, by assuming that the forward and spot market prices are already given. A detailed optimization framework of SMR and renewable based HES system included a district heating network model and focused only on a finer timescale (load-following and frequency regulation) operation.[22] Chen and Garcia[23] explored the market equilibrium between an electricity market and district heating market in a generalized single-stage market setup. A two-stage (day-ahead and real-time) integrated electricity and heat market clearing algorithm was proposed by Wang *et al.*,[24] where an economic dispatch problem was formulated in both stages rather than considering a unit-commitment model in the day-ahead market. Li *et al.*[25] analyzed the economic and environmental benefits of a small nuclear unit based isolated integrated energy system through the simulation of a single stage economic scheduling (dispatch) model. The model only includes the system-wide power balance constraints, unit specific capacity constraints, and spinning reserve constraints; the economic benefits are determined based on pre-defined fixed cost parameters instead of time-varying forward and spot market signals. Al Kindi *et al.*[26] assessed the operational benefits of a flexible nuclear plant based on a year-long simulation of a whole-electricity system investment model (WeSIM), where the whole system setup is represented by a single-node system without considering any network. Poudel and Gokaraju[27] developed dynamic models for small modular reactor (SMR) and district heating network (DHN) and performed simulations to study the transient response in a renewable based HES system setup. The work focused on the dynamic stability of the operation and assessed the contribution of N-R HES from the perspective of frequency response and load-following.

While many of the studies in the literature have proposed worthy and constructive operation strategies for the IES, most of the simulations have used a single-node system representation instead of using detailed grid models, which does not capture the detailed operational characteristics of individual system components. Moreover, most of the existing studies rely on pre-defined fixed cost parameters or historical electricity prices to measure the benefits of operation, rather than using the time-varying electricity prices at pricing points due to the limitation of lumped model simulation results. In addition, a majority of the studies have used a single-stage scheduling model to assess the operational benefits. Though a few studies have used a two-stage unit commitment-economic dispatch (UC-ED) structure, they have not adopted the required evolution of operational constraints. Regarding the thermal system simulation, existing models in the literature have only considered the capacity constraints and generation-load balance constraints, which is not sufficient to provide a comprehensive view on the physical properties of the sector-coupled thermal system.

To further explore the economic and reliability benefits of N-R HES, this work performs a detailed N-R HES operational study in a multi-timescale market environment by determining the market clearing price and dispatch levels simultaneously. In addition, a district heating network (DHN) is incorporated into the multi-timescale market model. The DHN is modeled as a lumped heating load constraint to be satisfied from the varying thermal power exhaust from the SMR. The bulk thermal dispatch is later fed into a detailed DHN model developed on a high-fidelity static analysis platform to check the feasibility of the solution in the thermal domain. A three-cycle production cost model is considered as the multi-timescale electricity market framework, where the participating cycles include a day-ahead security constrained unit commitment (DASCUC) model, a real-time security constrained unit commitment (RTSCUC) model, and a real-time security constrained economic dispatch (RTSCED) model. Components of the grid-tied N-R HES and the rest of the grid have been modeled in great detail to mimic the actual operational characteristics, e.g., ramp-rate constraints of generators at different stages of starting up and shutting down, reserve allocation, and deployment capacity constraints of generating units based on the reserve activation time and optimization horizon length, etc. Moreover, operational constraints have been modified at each timescale to facilitate the proper representation of the system components' response in different optimization horizons. The N-R HES components participate in providing different reserve products depending on their capability to respond within the respective reserve activation time. Instead of using a given price signal, the locational marginal price (LMP) is determined in each of the aforementioned cycles based on the interaction between N-R HES and the rest of the grid from the system-wide simulation. The N-R HES helps to satisfy the system-wide power and reserve requirements along with other generating entities through its electrical power and reserve dispatch, thereby actively participating in settling the LMPs at its pricing point. Major contributions of this work include

- A multi-timescale simulation and optimization framework for coupled electrical-district heating network is developed.
- The economic benefits of N-R HES are explored via participating in both energy and ancillary service markets and providing thermal products.
- The N-R HES is modeled to participate as a price-maker instead of a price-taker, allowing N-R HES to interact with the rest of the grid and affect the LMP.

The rest of the paper is organized as follows. Section II describes the model development and assumptions. Section III introduces the optimization models for multi-timescale electricity market simulations with N-R HES. Section IV presents a case study and results of N-R HES operations at different timescales. Conclusions and future work are discussed in Sec. V.

II. MODEL DEVELOPMENT AND ASSUMPTIONS

The N-R HES modeling and optimization framework are developed by leveraging the multi-timescale market models of the Flexible Energy Scheduling Tool for Integrating Variable Generation (FESTIV).[28] FESTIV allows for the explicit modeling of reserve allocation and deployment, unlike traditional production cost modeling which only accounts for the holding of reserves. While the base model of FESTIV only includes the detailed electrical system model, a lumped district heating network (DHN) model is added to the N-R HES site, enabling FESTIV to be a multi-carrier energy system simulator. The overall N-R HES setup is shown in Fig. 1.

A. Electrical model

While the multi-carrier energy system simulator platform could be applied to any general system, the electrical modeling is performed based on the NREL-118 system.[29] The electrical generators of N-R

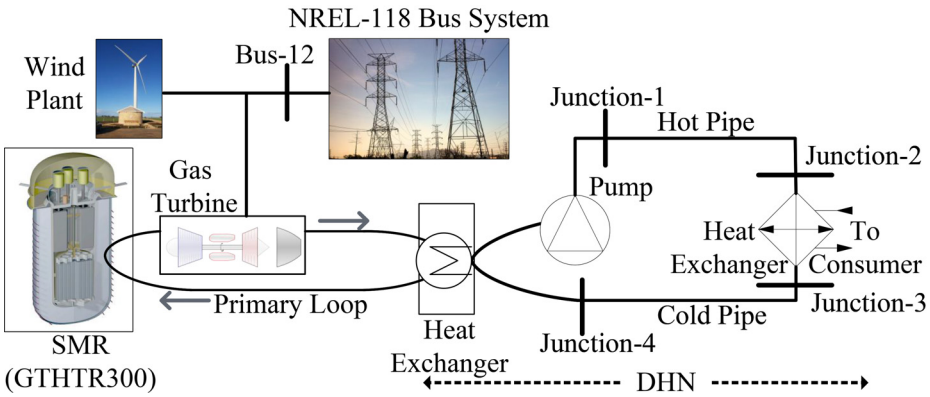

FIG. 1. The N-R HES with a DHN (modeled as a lumped thermal load), connecting to the NREL-118 system.

HES respond to the system demand and reserve requirement, by providing both energy and power products. The auxiliary consumption of the N-R HES is negligible, thus, excluded from the modeling. Therefore, there is no electrical load included within the N-R HES. To determine the optimal HES component ratings and location, simulations have been performed with different N-R HES component ratings at different buses with high load shares. By comparing the results obtained at all considered locations, bus-12 is selected for N-R HES installation, due to the least operational cost and the highest accommodation capability. More specifically, the N-R HES component ratings and location were selected through an empirical process by running the DASCUC model, where small modular reactors[30] and wind plants were placed at different load centers. By considering the convergence and objective function value, the best location (i.e., bus-12 in this case) was selected with the lowest total cost and reasonably rated N-R HES components (considering the district heating network demand satisfaction criterion). Detailed specifications of the N-R HES components (e.g., SMR, wind, etc.) are determined based on publicly available sources and literature.[31,32] In this study, the N-R HES consists of the following components:

- A small modular reactor of 320 MW_e capacity.
- A wind plant of 149.5 MW_e capacity.
- A 100 MW_t district heating load.

Reserve requirements are determined by following the default FESTIV reserve rule,[28] where the regulation reserve varies with the system load and other reserves are set at some fixed values. In this study, four types of reserves have been considered, namely, regulation reserves, spinning reserves, non-spinning reserves, and replacement reserves. The action hierarchy of these reserves is implemented by the difference in the value of insufficient reserves (VOIR) and their activation time. Renewable sources of N-R HES are only allowed to participate in the regulation reserve provision, while other generators' participation to provide different reserves is determined by their operational characteristics. The assumed VOIRs, their activation time, and system reserve requirements are summarized in Table I.

TABLE I. Reserve settings.

Reserve type	Activation time (min)	VOIR ($/MWh)	Reserve requirement (MW)
Regulation	5	7500	10% of total load
Spinning	10	5000	950
Non-spinning	10	1500	1900
Replacement	30	250	3000

B. District Heating Network (DHN) model

To better utilize the exhaust (process) heat from the nuclear plant of the N-R HES, a circular district heating network is connected via a 5-km long heat pipe with a standard loss factor. Generally, most of the technologies are not capable of using the exhaust heat from the nuclear plant without re-heating, but recently new technologies (e.g., GTHTR300)[33,34] can directly leverage the exhaust heat to provide a district heating load without compromising the electricity generation. Instead of using a steam turbine, this type of SMR uses a gas turbine that enables the waste heat rejection at a higher temperature, such as 200 °C.[33] In this work, the GTHTR300 SMR is employed to supply the DHN. The DHN is assumed to represent a city of sizable population of approximately 15 000 (a proportionate approximation from the heating load facts of the city of Paris, France)[35] with a maximum heating load of 100 MW_t.

The hydraulic and thermal modeling of the DHN is performed in pandapipes,[36] which is capable of modeling the hydraulic and thermal properties of different thermal systems in great detail. Pandapipes is a piping grid simulation tool, which is capable of simulating coupled multi-energy (e.g., power, gas, and district heating) grid infrastructure. Every component model in pandapipes is interpreted as nodes, edges of a network each connecting two nodes, and the node element. Equations are introduced to represent their physical properties. The set of equations comply with Kirchoff's laws. Jacobian matrices are derived for both hydraulic and heat transfer equations, which are eventually solved by the Newton–Raphson solver to obtain the hydraulic state variables and node temperatures for heating grids. The DHN model receives the thermal energy through a heat-exchanger that transfers the heat from the primary loop of the SMR to the heating fluid in the district heating circuit. This hot fluid is then circulated via a constant speed pump, and the thermal energy carried by the fluid is extracted by another heat-exchanger at the consumer end. The cold pipe carries the fluid back to the initial heat exchanger for reheating. The DHN model is developed based on the thermal and hydraulic characteristic equations.[37] At each of the junctions in the DHN model,

TABLE II. District heating network parameters.

Parameter	Value	Unit
Thermal conductivity of the heat pipe	53	W/(m K)
Diameter of the heat pipe	400	mm
Nominal pump and junction pressure	5	bar
Nominal outlet temperature of the primary loop heat exchanger	383.15	K
Nominal outlet temperature of the sink heat exchanger	343.15	K

the incoming and outgoing mass of heating element and thermal energy flows are balanced out according to the nodal rule of Kirchoff's law. Equations (1) and (2) represent the nodal mass and energy flow balance, respectively,

$$\sum_{e=1}^{N_e} \dot{w}_e + \dot{w}_n = \sum_{e=1}^{N_e} u_e A_e \rho_e + \dot{w}_n = 0, \tag{1}$$

$$\sum_{e=1}^{N_e} q_e = \sum_{e=1}^{N_{e,in}} \dot{w}_n c_p T_e - \sum_{e=1}^{N_{e,out}} \dot{w}_n c_p T_n = 0, \tag{2}$$

where $\dot{w}_e$ represents the mass flow of the heating fluid through edge e, and $\dot{w}_n$ represents the entering or outgoing fluid mass flow through node n, u_e denotes the flow velocity of the fluid, A_e denotes the cross-sectional area of the edge e (pipe), and ρ_e stands for the fluid density. q_e denotes the incoming and outgoing heat flow at node e, c_p represents the fluid heat capacity, and T_e and T_n represent the fluid and node temperature, respectively.The pressure and temperature differences Δp_e and ΔT_e in a closed loop follow Kirchoff's mesh rule, which are represented in the following equations:

$$\sum_{e=1}^{N_m} \Delta p_e = 0, \tag{3}$$

$$\sum_{e=1}^{N_m} \Delta T_e = 0, \tag{4}$$

where N_m denotes the number of edges (2 in this case) that constitute one closed loop. Since there is no height difference between the nodes (junctions), the pressure difference is calculated from the following equation:

$$\Delta p = -\frac{\rho \cdot u^2}{2} \cdot \left(\frac{\lambda}{d} \cdot \Delta l + \zeta\right), \tag{5}$$

where λ denotes the "Darcy friction factor," d is the pipe diameter, l is the pipe length, and ζ represents the pressure loss coefficient. The heating fluid velocity u is derived from the mass flow rate described in the following equation:

$$\dot{w} = \rho \cdot A \cdot u. \tag{6}$$

With reference to the aforementioned relations described in Eqs. (5) and (6), the pressure distribution $\frac{\Delta p}{\Delta l}$ is determined along the pipe length. For the heat transfer mode, the temperature gradient along the pipe length is determined by using the mass flow rate $\dot{w}$ calculated from the hydraulic equation [Eq. (6)] described above, which also takes into account the heat transfer with the external environment. The temperature distribution is represented in the following equation:

$$\dot{w} c_p \frac{\Delta T}{\Delta l} = -\alpha \cdot (T_{\text{external}} - T), \tag{7}$$

where α denotes the heat transfer coefficient and T_{external} denotes the external temperature. These characteristics equations are assembled as a set of non-linear equations and solved by the pandapipes solver. The DHN specifications for this study are adopted from the literature,[33] which are summarized in Table II.

To avoid dealing with the non-linearity in the DHN model, only the cumulative thermal load is considered as a parameter in the multi-timescale models, and the ex-post thermal dispatch amount is fed into the pandapipes DHN model (non-linear) to confirm the authenticity of the solution and obtain a detailed characteristics profile of the DHN. Figure 2 illustrates the process and data flow mechanisms of the proposed thermal–electric coupling framework by integrating FESTIV with pandapipes.

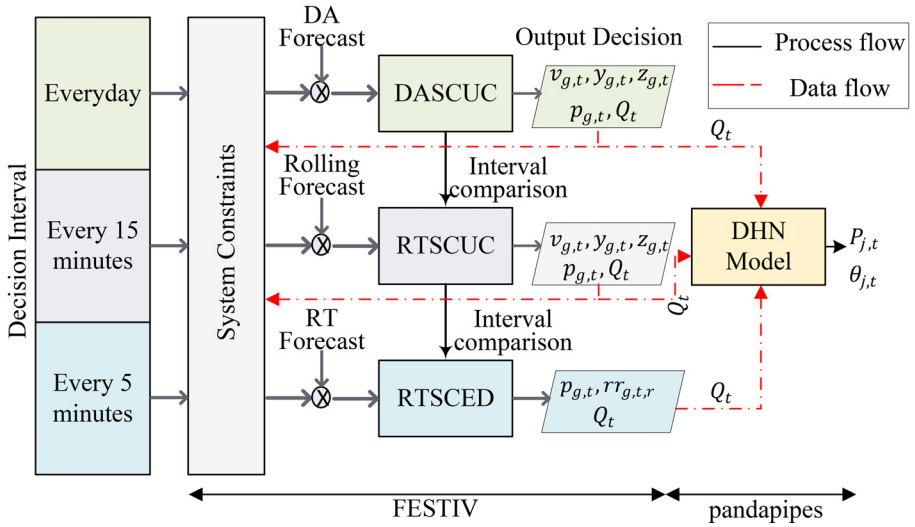

FIG. 2. High-level flow diagram for the proposed thermal-electric coupled IREM framework.

III. MULTI-TIMESCALE ELECTRICITY MARKET MODELING

The grid connected N-R HES is simulated in a three-cycle multi-timescale production cost modeling platform that replicates the whole time spectrum of scheduling and dispatch operations. The inter-temporal coupling of the sub-models within the multi-timescale framework is illustrated in Fig. 3. While N-R HES can provide a number of reserve and energy products at different timescales, this study develops optimization and control strategies to maximize the reserve export available from N-R HES, while satisfying their demand for the coupled thermal system. The developed framework, namely, the Integrated Reserve Export Maximization (IREM) Model, aims to maximize the reserve provision by N-R HES, thereby improving the economics of the system.

A. Integrated reserve export maximization model: DASCUC

In this IREM DASCUC model, the N-R HES operation is optimized to maximize the reserve export from N-R HES to the power grid in a forward market (i.e., 1 day-ahead at an hourly resolution). The optimization is performed in an integrated manner, where the interaction of N-R HES with the grid is reflected through system-level constraints, such as the bus power balance, total reserve requirement constraints, etc.; the same unit-specific constraints are applied to every component of the N-R HES to keep them consistent with other grid components. The day-ahead IREM model is formulated as follows (for brevity, some constraints are excluded; please refer to our previous study[15] for the detailed formulation).

1. Objective function and production cost constraints

$$\begin{aligned}\min \sum_{t\in T}\left[\sum_{g\in G}\left(su_{g,t}+sd_{g,t}+pc_{g,t}+\sum_{g\in G\setminus G_{HES}}\sum_{r\in RS}rc_{g,t,r}\right)+ls_t\right]\\ +\sum_{t\in T}\left[\sum_{r\in RS}VOIR_r ir_{t,r}+VOLL_{\text{thermal}}\times ll_{\text{thermal},t}\right]\\ -\sum_{t\in T}\sum_{g\in G_{HES}}\sum_{r\in RS}rc_{g,t,r},\end{aligned} \tag{8}$$

s.t.

$$su_{g,t}\geq SU_g[v_{g,t}-v_{g,t-1}],\quad \forall g\in G,\quad \forall t\in T, \tag{9}$$

$$sd_{g,t}\geq SD_g[v_{g,t-1}-v_{g,t}],\quad \forall g\in G,\quad \forall t\in T, \tag{10}$$

$$pc_{g,t}=NL_g v_{g,t}+\sum_{k=1}^{K_g}p_{g,t}^k C_g^k,\quad \forall g\in G,\quad \forall t\in T, \tag{11}$$

$$rc_{g,t,r}=\sum_{g\in G}rr_{g,t,r}RC_{g,r},\quad \forall g\in G,\quad \forall t\in T,\quad \forall r\in RS. \tag{12}$$

As shown in Eq. (8), the aggregated objective is to minimize the production cost of the whole system (represented by the first term), while maximizing the reserve cost ($rc_{g,t,r}$) of the N-R HES (represented by the third term). Unlike the usual unit commitment model formulation which is merely a production cost minimization model focusing on minimizing the cost components related to electrical power generation (including reserve costs) along with determining optimal commitment decisions for the plants. This deduction of N-R HES reserve cost enforces the maximum utilization of reserves exported from the N-R HES. The loss of thermal load is also penalized by a penalty factor $VOLL_{\text{thermal}}$, thereby implementing a soft constraint on the thermal load satisfaction requirement.

Equations (9) and (10) define the start-up ($su_{g,t}$) and shut-down ($sd_{g,t}$) costs, respectively. Equation (11) represents the production cost ($pc_{g,t}$) while considering the no-load costs (NL_g), and Eq. (12) defines the reserve cost ($rc_{g,t,r}$).

2. Maximum and minimum power output

$$P_g^{\min}v_{g,t}\leq p_{g,t}\leq \bar{p}_{g,t},\quad \forall g\in G,\quad \forall t\in T, \tag{13}$$

$$0\leq \bar{p}_{g,t}\leq P_g^{max}v_{g,t},\quad \forall g\in G,\quad \forall t\in T, \tag{14}$$

$$p_{g,t}=P_g^{\min}v_{g,t}+\sum_{k=1}^{K_g}p_{g,t}^k,\quad \forall g\in G,\quad \forall t\in T, \tag{15}$$

$$0\leq p_{g,t}^k\leq \Delta P_g^k,\quad \forall g\in G,\quad \forall t\in T, \tag{16}$$

$$P_g^{\min}v_{g,t}\leq p_{g,t}\leq P_{g,t}^{\text{forecast}},\quad \forall g\in G_{REN},\quad \forall t\in T. \tag{17}$$

Equations (13) and (14) limit the power output ($p_{g,t}$) of a unit in a particular period by the minimum power output ($p_g^{\min}$) and the maximum available power output ($\bar{p}_{g,t}$) (this is also constrained by the unit capacity ($p_g^{\max}$), respectively. Equations (15) and (16) implement the aggregated temporal output limit across all the generation cost blocks

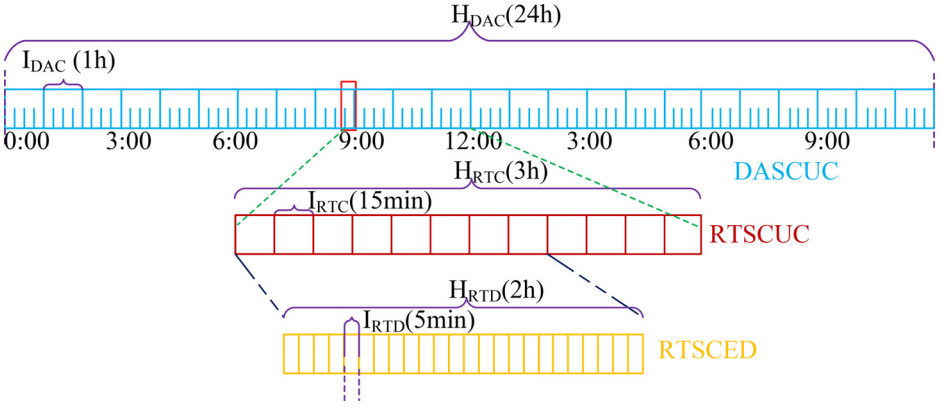

FIG. 3. The time-frame setup of three sub-models of IREM with their update interval and optimization horizon.

($p^k_{g,t}$). For renewable sources, the plant output is further constrained by its respective power forecast $P^{\text{forecast}}_{g,t}$ and the corresponding constraint is represented in Eq. (17).

3. Minimum up and down time constraints

$$\sum_{t=1}^{IUT_g}(1-v_{g,t})=0, \quad \forall g\in G, \tag{18}$$

$$\sum_{\tau=t}^{t+UT_g-1} v_{g,\tau}\geq UT_g(v_{g,t}-v_{g,t-1}), \quad \forall g\in G, \quad \forall t=IUT_g+1,\ldots,|T|-UT_g+1, \tag{19}$$

$$\sum_{\tau=t}^{T}\left[v_{g,\tau}-(v_{g,t}-v_{g,t-1})\right]\geq 0, \quad \forall g\in G, \quad \forall t=|T|-UT_g+2,\ldots,|T|. \tag{20}$$

Equation (18) enforces the generating units to retain their "ON" statuses if the unit is started at initial hours or before the optimization time horizon, but the minimum up time (UT_g) has still been in effect at the current time slot. Equation (19) represents the minimum up time constraint in effect after a transition from "OFF" to "ON" status change. Equation (20) ensures the continuous transition of unit status ($v_{g,t}$) at the end hours of the optimization horizon for units where minimum up time constraints are applicable. The constraints to enact minimum down time are similar to these and excluded for brevity.

4. Start-up and shut-down constraints

$$p_{g,t}\geq P^{\min}_g\left[v_{g,t}-\sum_{i=1}^{DD}z_{g,t+i}-\sum_{i=1}^{UD}y_{g,t-i+1}\right]+\sum_{i=1}^{UD}p^U_{g,i}y_{g,t-i+1}, \quad \forall g\in G, \quad \forall t\in T, \tag{21}$$

$$p_{g,t}\geq P^{\min}_g\left[v_{g,t}-\sum_{i=1}^{DD}z_{g,t+i}-\sum_{i=1}^{UD}y_{g,t-i+1}\right]+\sum_{i=1}^{DD}p^D_{g,i}z_{g,t+DD-i+1}, \quad \forall g\in G, \quad \forall t\in T, \tag{22}$$

$$p_{g,t}\leq P^{\min}_g\left[v_{g,t}-\sum_{i=1}^{UD}y_{g,t-i+1}\right]+\sum_{i=1}^{UD}p^U_{g,i}y_{g,t-i+1}, \quad \forall g\in G, \quad \forall t\in T, \tag{23}$$

$$p_{g,t}\leq P^{\min}_g\left[v_{g,t}-\sum_{i=1}^{DD}z_{g,t+i}\right]+\sum_{i=1}^{DD}p^D_{g,i}z_{g,t+DD-i+1}, \quad \forall g\in G, \quad \forall t\in T, \tag{24}$$

$$y_{g,t}-z_{g,t}=v_{g,t}-v_{g,t-1}, \quad \forall g\in G, \quad \forall t\in T, \tag{25}$$

$$v_{g,t}\geq\sum_{i=1}^{UD}y_{g,t-i+1}, \quad \forall g\in G, \quad \forall t\in T, \tag{26}$$

$$v_{g,t}\geq\sum_{i=1}^{DD}z_{g,t+i}, \quad \forall g\in G, \quad \forall t\in T. \tag{27}$$

Equations (21) and (22) represent the lower limits for a unit's start-up and shut-down trajectories, respectively. *UD* and *DD* denote the start-up and shut-down time, respectively; $p^U_{g,i}$ and $p^D_{g,i}$ represent generator's power output at the starting and shut-down period, respectively. They also bound the ramp-up and ramp-down limits for the particular period. For both start-up and shut-down processes, the first term on the right hand side becomes ineffective and the second term of both Eqs. (21) and (22) effectively controls the start-up and shut-down power trajectory. Similar to Eqs. (21) and (22), (23) and (24) set the maximum limit of the power trajectories for the start-up and shut-down process, respectively. Equation (25) denotes the shut-down and start-up status change constraint. The parameters $y_{g,t}$, and $z_{g,t}$ denote the starting up and shutting down statuses, respectively. Equations (26) and (27) ensure that the unit is online while starting-up or shutting-down, respectively.

5. Reserve constraints

$$\bar{p}_{g,t}-\sum_{r\in RS}rr_{g,t,r}\leq p_{g,t-1}+R^U_g v_{g,t-1}+R^{SU}_g[v_{g,t}-v_{g,t-1}]+P^{\max}_g(1-v_{g,t}), \quad \forall g\in G, \quad \forall t\in T, \quad \forall r\in RS, \tag{28}$$

$$p_{g,t}+\sum_{r\in RS}rr_{g,t,r}\leq\bar{p}_{g,t}, \quad \forall g\in G, \quad \forall t\in T, \quad \forall r\in RS. \tag{29}$$

Equation (28) enforces the satisfaction of the reserve requirements while respecting the ramping capability. The parameter R^U_g denotes the regular ramp-up rate of the unit, and R^{SU}_g denotes the ramp-up rate at the time of starting up. A similar reserve constraint has also been used to implement the limit for the ramp-down process. Equation (29) ensures the reserve provision from the unit's available capacity.

6. Ramping constraints

$$\bar{p}_{g,t}\leq R^{SD}_g[v_{g,t}-v_{g,t+1}]+P^{\max}_g v_{g,t+1}, \quad \forall g\in G, \quad \forall t=1,\ldots,|T|-1, \tag{30}$$

$$p_{g,t-1}-p_{g,t}\leq R^D_g v_{g,t}+R^{SD}_g(v_{g,t-1}-v_{g,t})+P^{\max}_g(1-v_{g,t-1}), \quad \forall g\in G, \quad \forall t\in T, \tag{31}$$

$$p_{g,t}-p_{g,t-1}\leq P^{\min}_g\sum_{i=1}^{UD}y_{g,t-i+1}+R^U_g\left[v_{g,t}-\sum_{i=1}^{UD}y_{g,t-i+1}\right], \quad \forall g\in G, \quad \forall t\in T, \tag{32}$$

$$p_{g,t-1}-p_{g,t}\leq P^{\min}_g\sum_{i=1}^{DD}z_{g,t+i-1}+R^D_g\left[v_{g,t-1}-\sum_{i=1}^{DD}z_{g,t+i-1}\right], \quad \forall g\in G, \quad \forall t\in T. \tag{33}$$

Equation (30) represents the constraint required to determine the available power output of an unit at the time of status transition. Equation (31) represents the ramping constraint at the intervals of unit status transitions where the ramping profile is restricted by the corresponding active upper limit. Equation (32) implements the ramp-up limit for all intervals except the start-up period. Equation (33) represents the ramp-down limit at times of shutdown.

7. System level constraints

$$\sum_{g\in G} p_{g,t} - \sum_{b\in B_L} D_{b,t} - \sum_{b\in B_L} \delta_{b,t} = 0, \quad \forall t \in T, \tag{34}$$

$$p_{b,t}^{\text{net}} = \sum_{g\in G\setminus G_{HES}} p_{b,g,t} IF_{b,g} - D_{b,t} + \delta_{b,t} + \begin{cases} \sum_{g\in G_{HES}} p_{b,g,t}, & \forall b \in B_{HES}, \quad \forall t \in T \\ 0, & \text{otherwise}, \end{cases} \tag{35}$$

$$\delta_{b,t} \le D_{b,t}, \quad \forall b \in B_L, \quad \forall t \in T, \tag{36}$$

$$\sum_{g\in G} rr_{g,t,r} + ir_{t,r} \ge RRR_{t,r}, \quad \forall t \in T, \quad \forall r \in RS, \tag{37}$$

$$rr_{g,t,reg} \le R_g^{U|D}, \quad \forall g \in G, \quad \forall t \in T, \tag{38}$$

$$lf_{l,t} = \sum_{b\in B} PTDF_{l,b} p_{b,t}^{\text{net}}, \quad \forall l \in L, \quad \forall t \in T, \tag{39}$$

$$-\text{Limit}_l \le \text{lf}_{l,t} \le \text{Limit}_l, \quad \forall l \in L, \quad \forall t \in T, \tag{40}$$

$$\eta \times p_{g(\text{nuclear}),t} + ll_{\text{thermal},t} \ge D_{\text{thermal},t}, \quad \forall t \in T. \tag{41}$$

Equations (34)–(41) represent system level constraints. Equation (34) is the system energy balance constraint. The parameter ($D_{b,t}$) represents the bus load, and $\delta_{b,t}$ represents the shedded load. Equation (35) is the bus-wise net energy constraint, and ($IF_{b,g}$) represents the bus injection factor. The bus-wise net energy constraint has been modified to accommodate the net power export ($p_{b,g,t}$) from the N-R HES at the point of common coupling bus. Equation (36) represents the load-shedding limit constraint. Equations (37) and (38) represent the reserve constraints. Line flows ($\text{lf}_{l,t}$) are calculated by using the power transfer distribution factor (PTDF) matrix in Eq. (39) and their limits (Limit_l) are enforced by Eq. (40). Equation (41) incorporates the district heating load ($D_{\text{thermal},t}$) satisfaction requirement constraint in the model, where the thermoelectric conversion efficiency (η) is assumed to be 33%, and a quarter of the energy is assumed to be carried by the waste heat rejected by the SMR. This is an overly relaxed assumption compared to Ref. 33 which envisions a deployment of higher efficiency reactor. The district heating load constraint is modeled as a soft constraint to allow the asynchronous dispatch of the thermal fluid.[38]

B. Integrated reserve export maximization model: RTSCUC

Within the hierarchy of the multi-timescale simulation framework, the real-time unit commitment model is run ahead of the real-time economic dispatch. In this work, the RTSCUC model is run at a 15-min interval. Commitment decisions can only be different than the DASCUC results if the minimum-up time, down time, start-up, and shut-down time of a specific plant comply with the time interval of RTSCUC simulations. Since this is also a unit commitment model, most of the optimization constraints are similar to the DASCUC model, whereas the commitment status from either the DASCUC or immediate previous RTSCUC simulation results are passed on as the initial commitment status. The objective function of RTSCUC is exactly same to the DASCUC objective function but with a different interval length. Since most of the constraints are similar to those in the DASCUC model, only the constraints with significant differences are included here for the sake of brevity,

$$y_{g,t} - z_{g,t} = v_{g,t} - v_{g,|T|}, \quad \forall g \in G, \quad \forall t = 1, \tag{42}$$

$$y_{g,\text{real}} - z_{g,\text{real}} = v_{g,t} - v_{g,\text{real}}, \quad \forall g \in G, \quad \forall t = 1, \tag{43}$$

$$y_{g,|T|} - z_{g,|T|} = v_{g,|T|} - v_{g,\text{real}}, \quad \forall g \in G. \tag{44}$$

Equations (42)–(44) reflect the commitment constraints of the generating units (the subscript "real" represents the actual status value obtained from the latest cycle). This illustrates how the unit commitment decisions are dictated by the previous cycle decisions and propagated from one cycle to the next immediate cycle.

Equations (45) and (46) ensure the compliance of minimum capacity constraints of the generators, and Eq. (47) represents the generator ramping constraints,

$$\begin{aligned} &p_{g,t} - \sum_r rr_{g,t,r} \\ &\ge p_g^{\min}\left[v_{g,t} - \sum_{t=t}^{t+TDP_g-1} z_{g,t} - \sum_{t-TUP_g+1}^{t=t} z_{g,t}\right] \\ &+ p_g^{\min} \times \min(1, I_{RTC}/UD_g)\left[\sum_{i=t-TUP_g+1}^{t} (t-i+1) \times y_{g,i}\right] \\ &+ p_g^{\min} \times \min(1, I_{RTC}/DD_g)\left[\sum_{i=t}^{t+TDP_g-1} (i-t) \times z_{g,i}\right], \\ &\forall g \in G, \quad \forall t \in [\text{TUP}_g - \text{ISA}_g, H_{RTC} - \text{TDP}_g] \end{aligned} \tag{45}$$

$$\begin{aligned} &p_{g,t} - \sum_r rr_{g,t,r} \\ &\ge p_g^{\min}\left[v_{g,t} - \sum_{t=t}^{H_{RTC}} z_{g,t} - \sum_{t=t-TUP_g+1}^{t} y_{g,t}\right] \\ &+ p_g^{\min} \times \min(1, I_{RTC}/UD_g)\left[\sum_{i=t-TUP_g+1}^{t} (t-i+1) \times y_{g,i}\right] \\ &+ p_g^{\min} \times \min(1, I_{RTC}/DD_g)\left[\sum_{i=t}^{H_{RTC}} (i-t) \times z_{g,i}\right], \\ &\forall g \in G, \quad \forall t \in \left[\max(H_{RTC} - TDP_g, TUP_g - ISA_g - 1), H_{DAC}\right] \end{aligned} \tag{46}$$

$$\begin{aligned} &p_{g,t} - p_{g,t-1} \\ &\le R_g^U \times I_{RTC} \times \left[v_{g,t} - PSCS_g - y_{g,|T|} - \sum_{t=1}^{t} y_{g,t}\right] \\ &+ p_g^{\min} \times \left(\frac{I_{RTC}}{UD_g}\right) \times (PSCS_g + y_{g,|T|} + \sum_{t=1}^{t} y_{g,t}), \\ &\forall g \in G, \quad \forall t \in [1, TUP_g - ISA_g]. \end{aligned} \tag{47}$$

C. Integrated reserve export maximization model: RTSCED

The RTSCED model is simulated at a 5-min interval. Thus, within each real-time unit commitment optimization horizon, the

RTSCED model is run three times. The commitment status from the RTSCUC model is passed to the RTSCED model. The RTSCED model determines the dispatch level of the generating units, so the dispatch results of the unit commitment models and the RTSCED model may differ in magnitude. Other than the commitment related constraints, the RTSCED model also contains similar constraints that affect the real-time economic operations of the system. Equation (48) implements the maximum capacity limit of the generating units, whereas the generator minimum capacity limits are imposed through Eq. (49),

$$p_{g,t} + \sum_{r} rr_{g,t,r} \le p_g^{\max}(v_{g,t} - z_{g,t}) + z_{g,t} \times \min\left[p_g^{\min}, \left(\prod_{t=t}^{H_{RTD}} z_{g,t}\right) + \sum_{t=t}^{H_{RTD}} \left(v_{g,t} \times z_{g,t} \times p_g^{\min} \times \frac{I_{RTD}}{TD_g}\right)\right], \quad \forall g \in G, \quad \forall t \in T \tag{48}$$

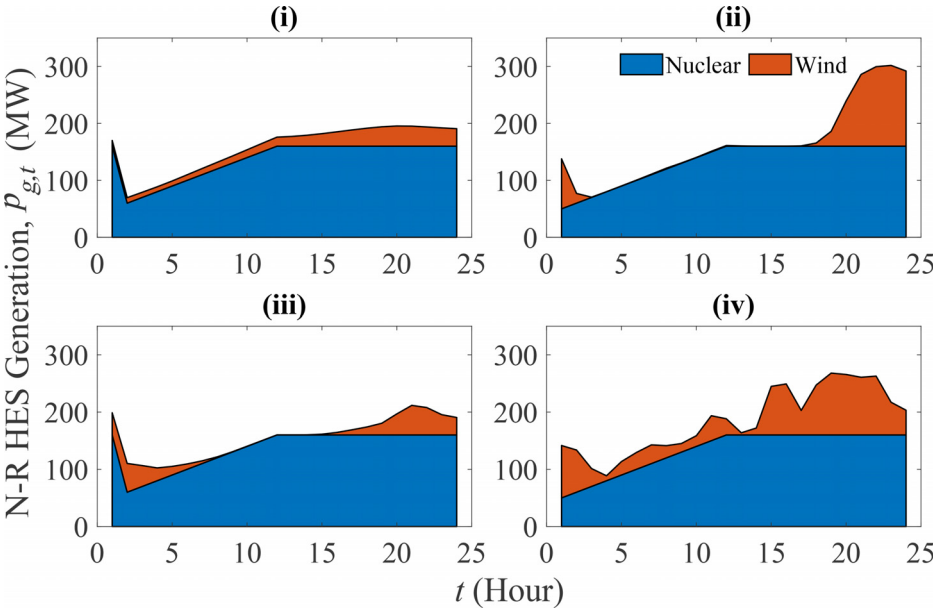

FIG. 4. Comparison with seasonal variation: electrical power generation of the nuclear and wind plants in the N-R HES in the DA cycle of a typical day in (i) January, (ii) April, (iii) July, and (iv) October.

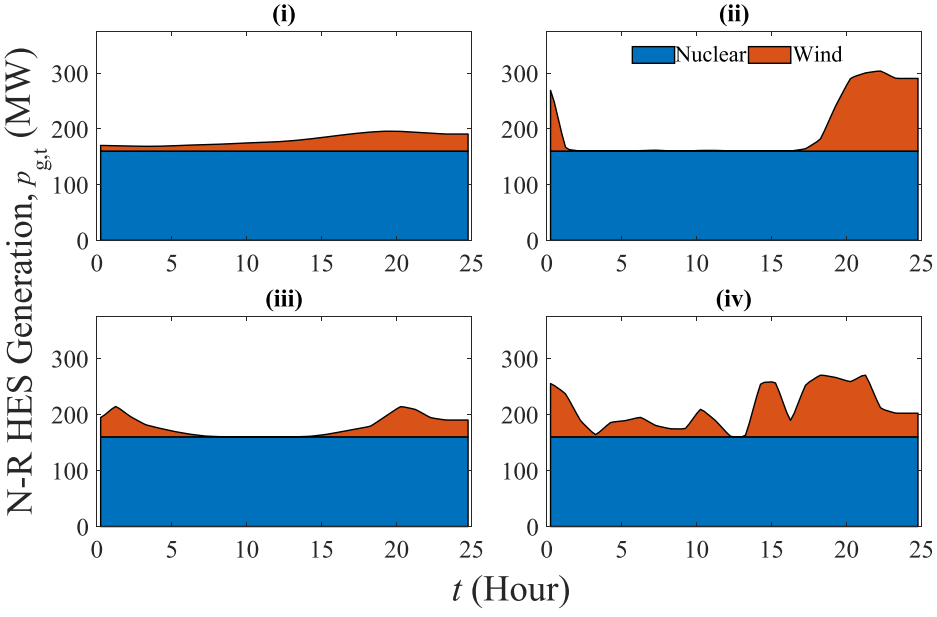

FIG. 5. Comparison with seasonal variation: electrical power generation of the nuclear and wind plants in the N-R HES in the RTSCUC cycle of a typical day in (i) January, (ii) April, (iii) July, and (iv) October.

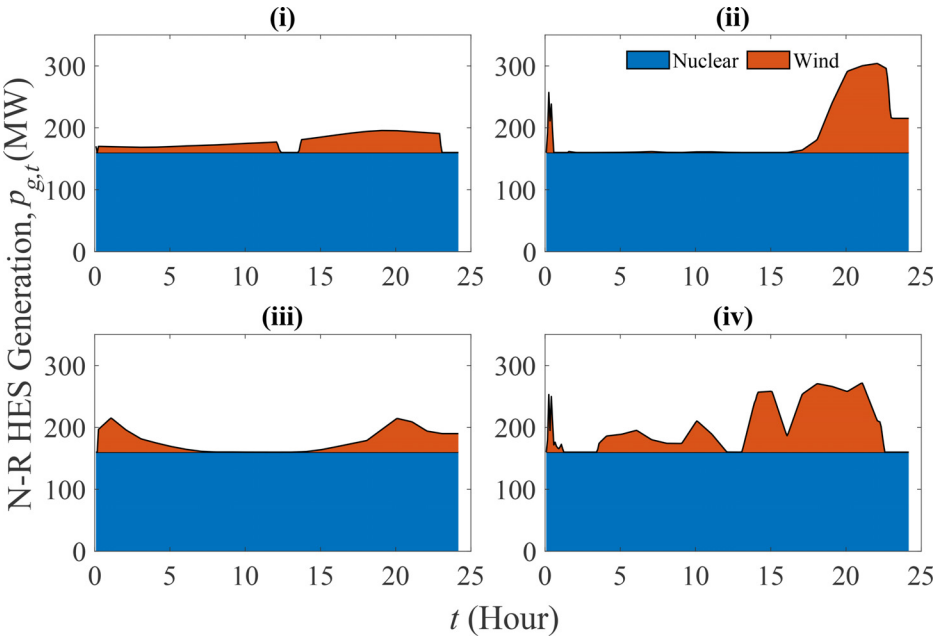

FIG. 6. Comparison with seasonal variation: electrical power generation of the nuclear and wind plants in the N-R HES in the RTSCED cycle of a typical day in (i) January, (ii) April, (iii) July, and (iv) October.

$$p_{g,t} - \sum_{r} rr_{g,t,r} \geq p_g^{\min}(v_{g,t} - z_{g,t} - y_{g,t}) + y_{g,t} \times \min\left[p_g^{\min}, \left(\prod_{t=1}^{t} y_{g,t}\right) + \sum_{t=1}^{t=t}\left(y_{g,t} \times p_g^{\min} \times \frac{I_{RTD}}{UD_g}\right)\right]$$
$$+ z_{g,t} \times \left(p_g^{\min} - \left[\min\left(p_g^{\min}, \left(\prod_{t=t}^{H_{RTD}} z_{g,t}\right) + \sum_{t=t}^{H_{RTD}}\left(v_{g,t} \times z_{g,t} \times p_g^{\min} \times \frac{I_{RTD}}{TD_g}\right)\right]\right)\right), \quad \forall g \in G, \quad \forall t \in T. \tag{49}$$

IV. CASE STUDY AND RESULTS

A. Experimental setup

The NREL-118 system is adopted and modified due to its high renewable penetration. There are 17 wind farms (approximately 4.38% installed capacity share) and 75 photovoltaic (PV) plants (approximately 14% installed capacity share) in the system. The N-R HES was added to a particular bus of the NREL-118 system, which is determined empirically. For the district heating load profile, the data

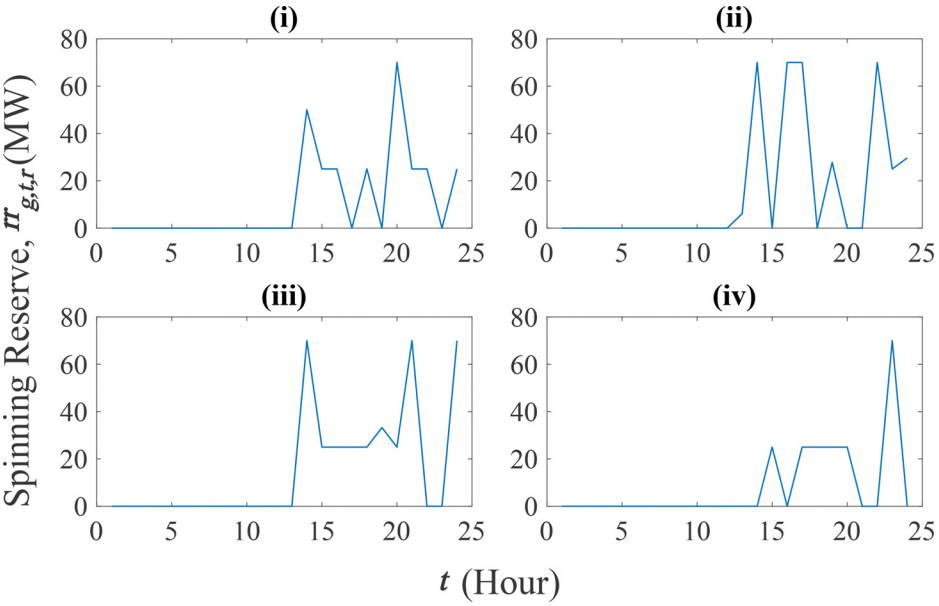

FIG. 7. Spinning reserve from N-R HES in the DA cycle of a typical day in (i) January, (ii) April, (iii) July, and (iv) October.

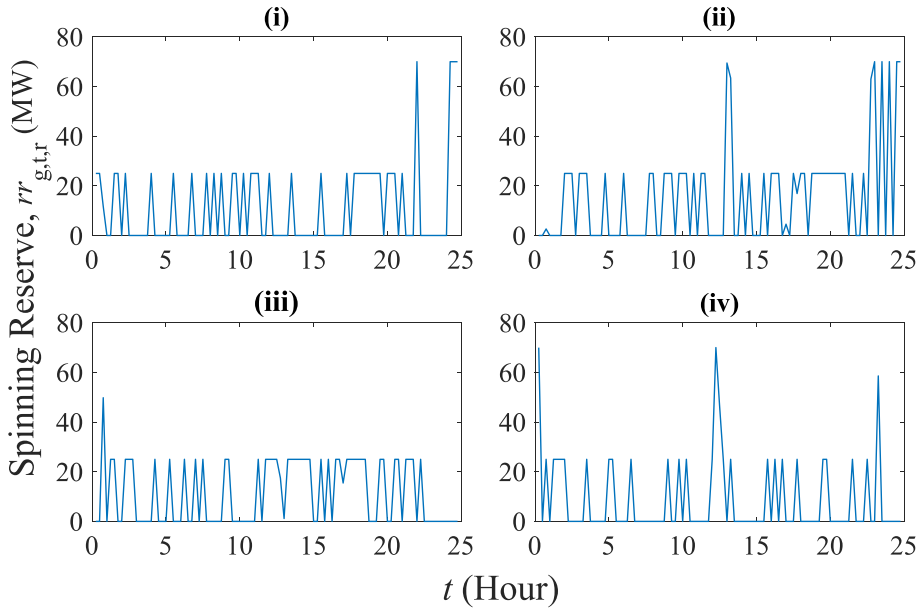

FIG. 8. Spinning reserve from N-R HES in the RTSCUC cycle of a typical day in (i) January, (ii) April, (iii) July, and (iv) October.

provided in the Dispa-SET[39] repository have been adopted but scaled down by assuming a 100 MW_t maximum capacity. Since the multi-timescale model simulations (DASCUC, RTSCUC, and RTSCED) require renewable power and load forecasts, both day-ahead forecasts and real-time forecasts from the NREL-118 bus system repository are adopted.[40]

To explore the impact of seasonal variation in the electrical and thermal load on the N-R HES operation and corresponding electricity market, the whole system is simulated in the multi-timescale environment for a 24-h period for four typical days, i.e., one from each season of the year (electrical load data for the first day of January, April, July, and October from the NREL-118 bus test system's year-2024 data repository[40] and thermal load data for the same days from Dispa-SET[39] data repository). Simulations are restricted to only a single day-time horizon due to the high computational expense to solve the models. The three-cycle models are formulated in GAMS 32.2 and solved by ILOG CPLEX 12.8. All the simulations are performed on a high performance computing facility (Ganymede[41]) using 40 processors and 64-GB memory. The input and output data processing is performed using the MATLAB interface of FESTIV. The thermal dispatch data are post-processed via a GAMS-pandapipes interface using the embedded code option of GAMS. The thermal load dispatch is

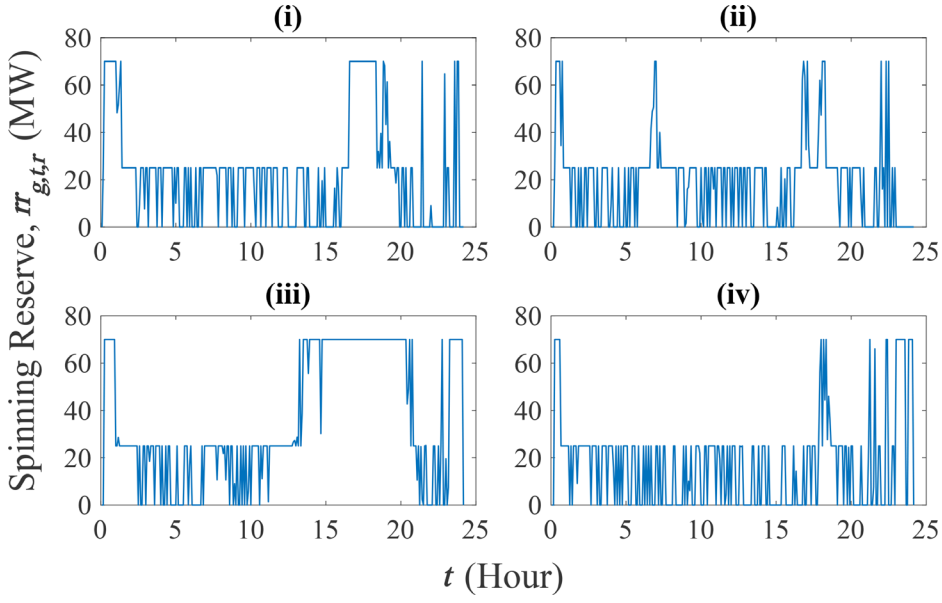

FIG. 9. Spinning reserve from N-R HES in the RTSCED cycle of a typical day in (i) January, (ii) April, (iii) July, and (iv) October.

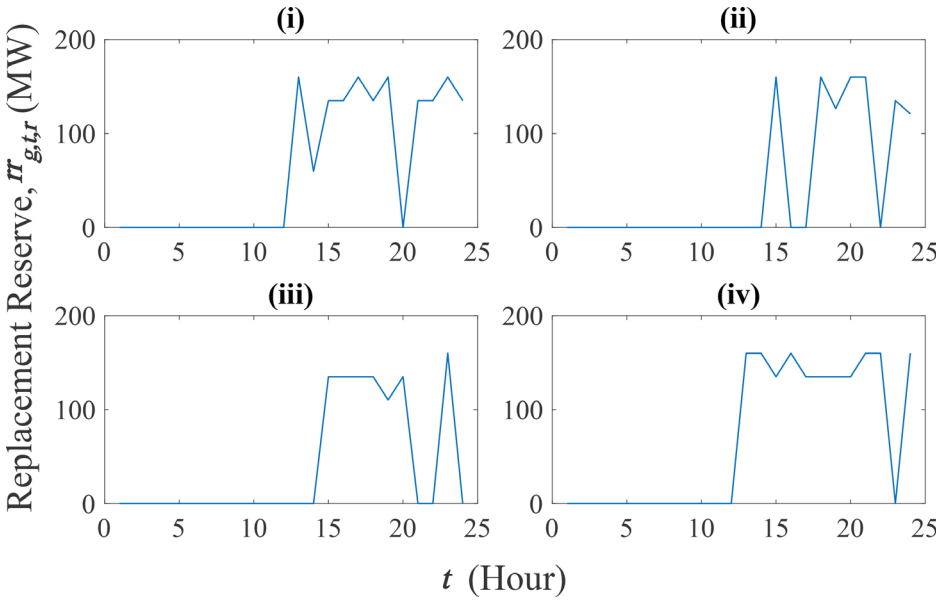

FIG. 10. Replacement reserve from N-R HES in the DA cycle of a typical day in (i) January, (ii) April, (iii) July, and (iv) October.

converted to a proportional mass flow rate to be fed into the pandapipes hydraulic-thermal model of the DHN. The nominal mass flow rate for the maximum SMR generation is set at 60 kg/s, which is proportionally changed based on the electrical output of the SMR. To provide the considered thermal load with realistic network parameters, it is assumed that 10 identical DHNs are connected to the SMR heat exhaust section.

B. Results and discussion

This study investigates the whole system energy resource scheduling and dispatch in DASCUC, RTSCUC, and RTSCED cycles in typical days of the four seasons. Since the 10 connected DHNs are identical, the day-ahead (DA) pressure and temperature profiles are presented for one representative DHN.

Figure 4 illustrates the day-ahead generation from N-R HES at a typical day in four different seasons of the year. The N-R HES demonstrates its responsiveness to the system load, as the cumulative N-R HES generation increases at late peak hours of the day. The N-R HES cumulative generation profile in October has a higher variation compared to others, due to the more variable wind generation. Figures 5 and 6 show the N-R HES generation obtained from the RTSCUC and RTSCED cycles, respectively. The same trend of generating more

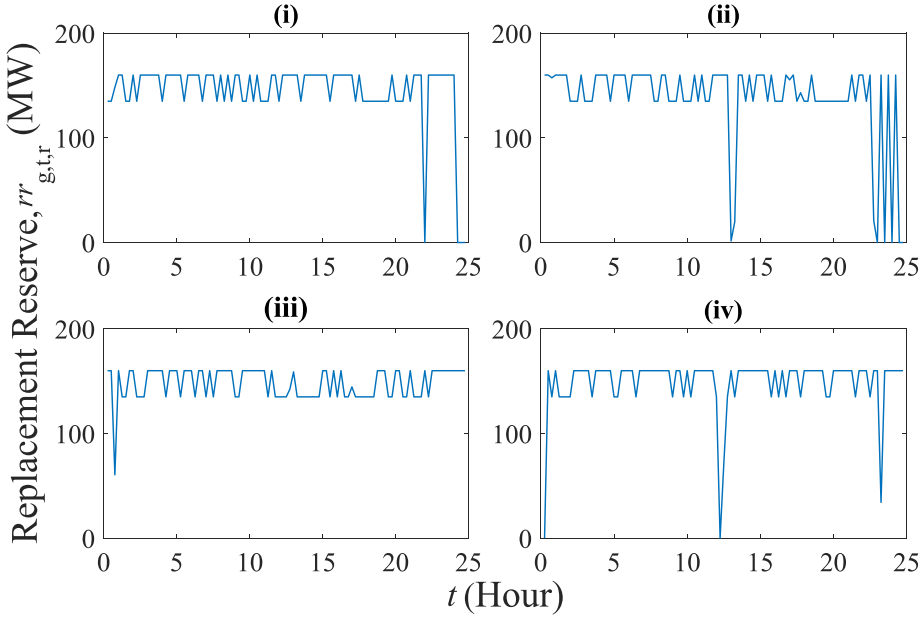

FIG. 11. Replacement reserve from N-R HES in the RTSCUC cycle of a typical day in (i) Januray, (ii) April, (iii) July, and (iv) October.

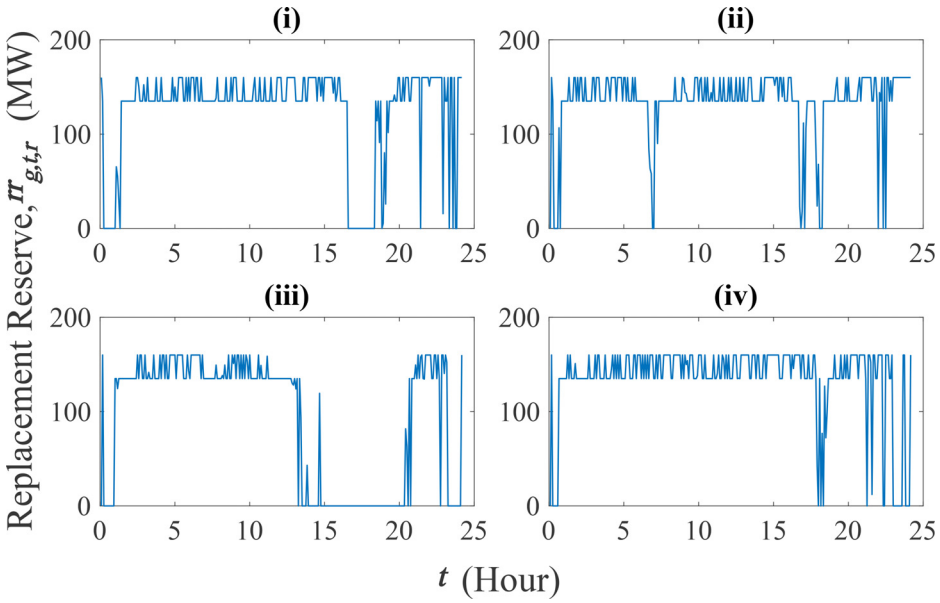

FIG. 12. Replacement reserve from N-R HES in the RTSCED cycle of a typical day in (i) January, (ii) April, (iii) July, and (iv) October.

power at the late peak hours can also be seen here, though with a higher granularity in the RTSCUC and RTSCED cycles. Compared to the DA cycle, the nuclear power output remains flat at all intervals since ramping becomes prohibitive in the shorter optimization horizon in the real-time cycles due to its slower ramp-rate. The nuclear plant prefers to capitalize its power over other ancillary products. The wind plant shows slightly different profiles in these cycles. The RTSCUC has more wind generation than the RTSCED, as the RTSCED time resolution is more suitable for the wind plant to allocate its capacity for more expensive ancillary services.

Figures 7–9 show the spinning reserve schedules from N-R HES in both day-ahead and real-time cycles. Akin to the generation schedule, the real-time schedules show more variability due to the higher time resolution, thus allowing more frequent changes in scheduling decisions. The non-spinning reserve is also included in the reserve spectrum, but since the objective aims to the maximum utilization of N-R HES resources to ensure the maximum return on the investments made on this capital intensive energy source, units switching from offline to online status were not observed within the simulation. Thus, N-R HES did not contribute to the non-spinning reserve during the simulation periods.

Figures 10–12 show the contribution of N-R HES to the replacement reserve requirement in both day-ahead and real-time cycles. A similar pattern of more variability in the real-time cycles is also

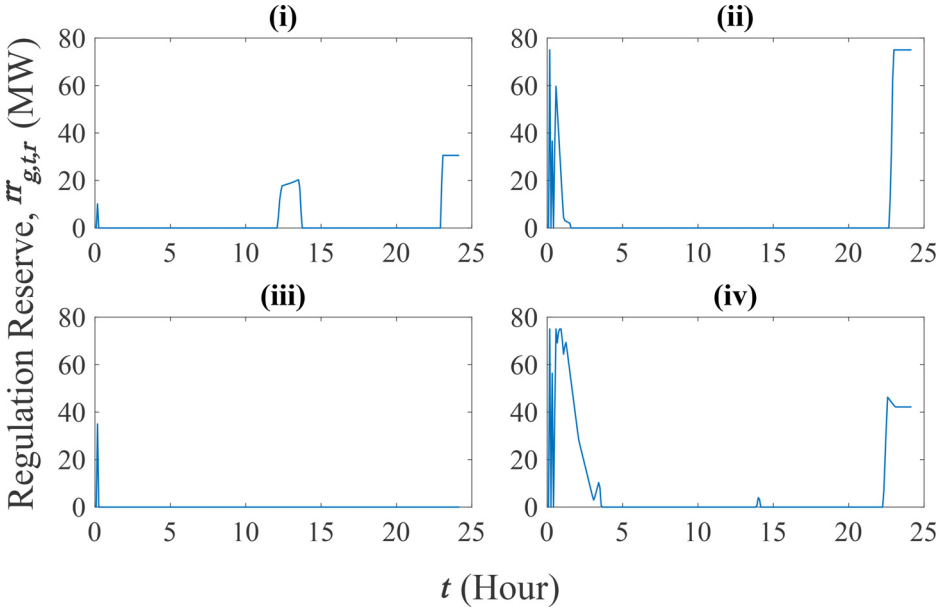

FIG. 13. Regulation reserve from N-R HES in the RTSCED cycle of a typical day in (i) January, (ii) April, (iii) July, and (iv) October.

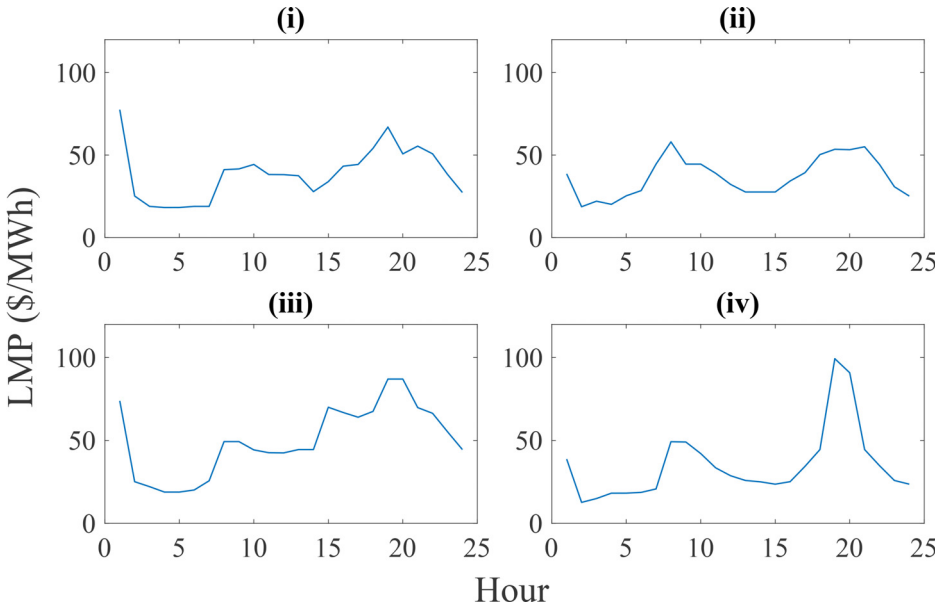

FIG. 14. DA LMP at the N-R HES location of a typical day in (i) January, (ii) April, (iii) July, and (iv) October.

observed in the replacement reserve schedules from N-R HES, but the magnitude is higher than that of the other reserve products. The replacement reserve has a longer activation time than others, so less flexible plants like nuclear plants are expected to participate more in replacement reserve provision. While the nuclear plant in the N-R HES is chosen to participate in all types of reserve products, the wind plant is only included in the regulation reserve provision.

Figure 13 shows the regulation reserve schedules of N-R HES in the RTSCED cycle. In the day-ahead and RTSCUC cycles, none of the N-R HES components is observed to participate in the regulation reserve provision. The reserved wind generation capacity during the RTSCUC cycle is dispatched as regulation reserve in the RTSCED cycle, since the regulation reserve activation time properly aligns with the RTSCED optimization horizon length. Due to the inclusion of reserve products from N-R HES in all three market models, part of the N-R HES capacity is allocated for reserve provision.

The locational marginal prices (LMPs) of the electric system from the DASCUC, RTSCUC, and RTSCED models at the N-R HES location are shown in Figs. 14–16, respectively. Compared to the DASCUC and RTSCED cycles, RTSCUC has higher LMPs. The reason can be attributed to the costs associated with starting up and shutting down a larger number of fast but expensive units. This leads to

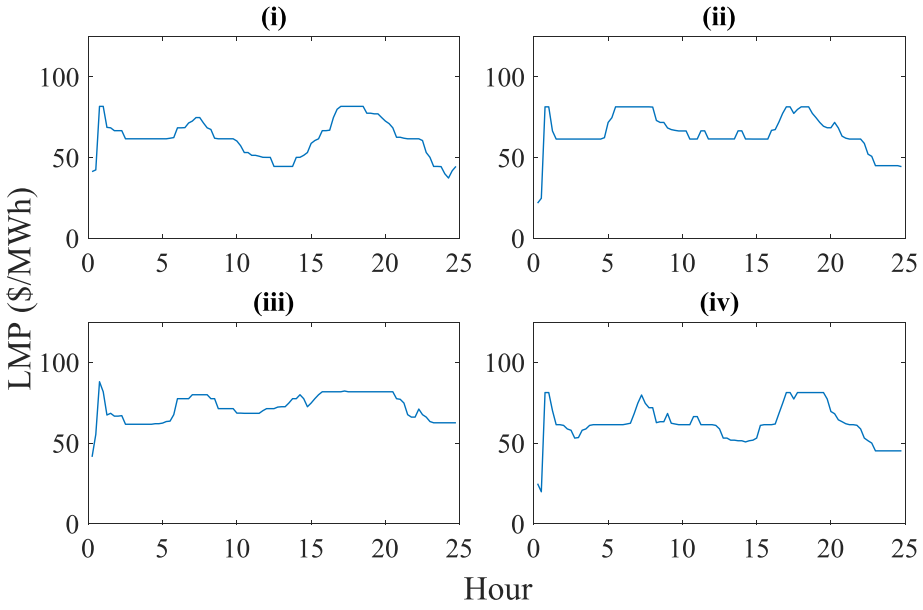

FIG. 15. RTSCUC LMP at the N-R HES location of a typical day in (i) January, (ii) April, (iii) July, and (iv) October.

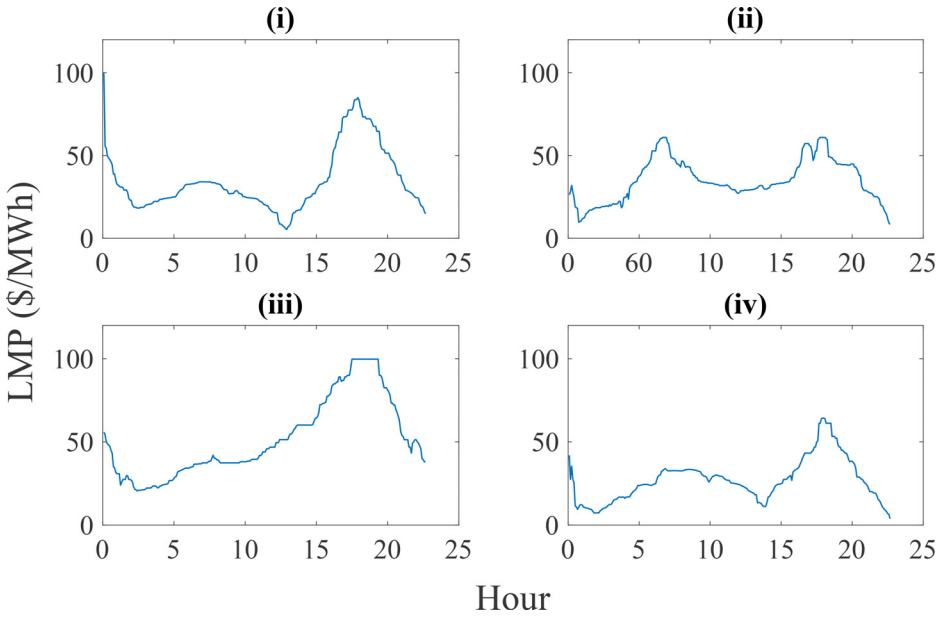

FIG. 16. RTSCED LMP at the N-R HES location of a typical day in (i) January, (ii) April, (iii) July, and (iv) October.

higher operating cost and results in a comparatively higher marginal cost value compared to DASCUC (in which slower plants are committed) and RTSCED (that does not take into account of no load, start-up, and shut-down costs). Higher N-R HES generation can also lead to higher LMPs, due to potential congestion cost increase as a result of higher power injection from N-R HES. When the congestion cost component of the LMP is increased due to this surplus injection, the energy costs are also affected, as the branches connected to the N-R HES bus have capacity limits. So accommodating additional generation and reserve allocation from N-R HES may lead to costly adjustments of the dispatch level of expensive online units. Since there exist complex interactions among system components in calculating the LMP, it is challenging to exactly pinpoint the LMP causes.

The DHN thermal load and the loss of load in the day-ahead cycle are shown in Fig. 17. An instance of loss of thermal load is observed in January, which is the coldest month with the highest heating load. In other months of the year and in real-time cycles, there is no loss of load observed. These thermal load loss profiles implicitly imply that the N-R HES is solely capable of meeting the thermal load demand in most instances.

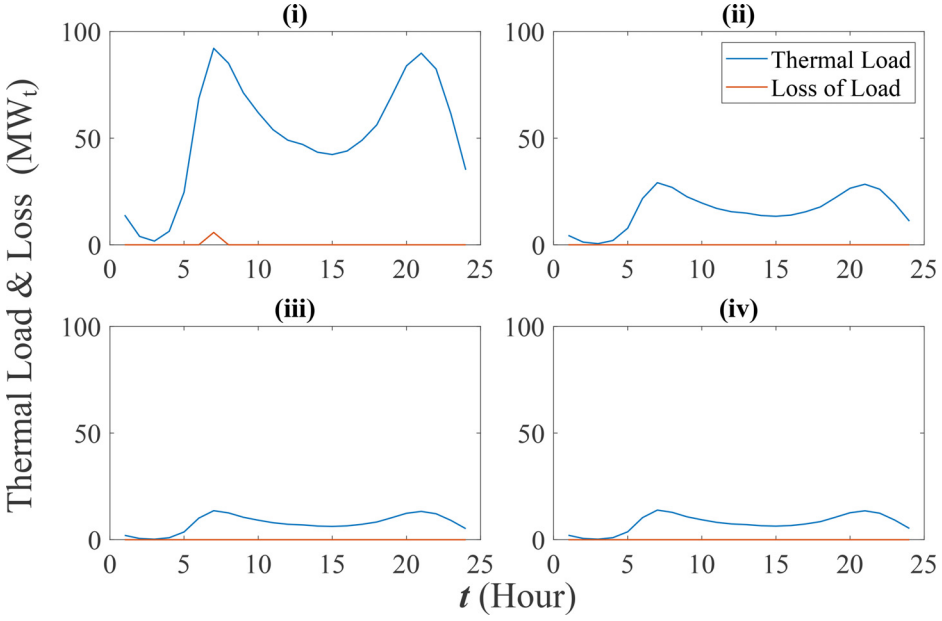

FIG. 17. Thermal load profiles of DHN in the DA cycle of a typical day in (i) January, (ii) April, (iii) July, and (iv) October.

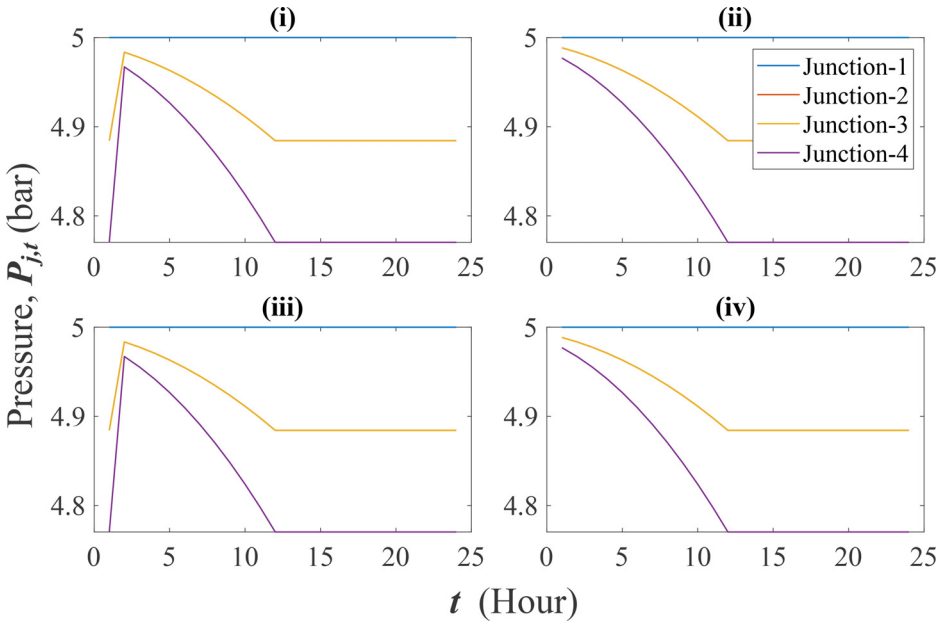

FIG. 18. Pressure profiles of the DHN in the DA cycle of a typical day in (i) January, (ii) April, (iii) July, and (iv) October. (Pressure profiles of Junction-2 are same to Junction-3 pressure profiles in all cases.).

The pressures at four junctions in the DHN are shown in Fig. 18, which are determined from the pandapipes simulation of the DHN, with given thermal load dispatch schedules in the day-ahead cycle. Since the real-time simulation results are very similar to the DA results, they are not included here. It is evident that all the junction pressures are around the nominal 5 bar pressure setpoint. Junction-2 and Junction-3 show the same pressure profile at all the intervals due to their close proximity. Junction 4 shows the most drastic change due to its proximity to the end of the return cold pipe.

The temperature profile along the DHN is summarized in Table III. The temperature profile remains the same in all of the simulated days and in other cycles. The temperature values at different junctions are close to the nominal setpoints and are within the acceptable range.

To assess the economic benefits of the proposed reserve maximization approach, a baseline case is designed, where the reserve export is not maximized and the waste heat of N-R HES is not utilized. Figure 19 compares the N-R HES revenue between the proposed IREM framework (with reserve optimization and district heating supply) and the baseline, in the day-ahead unit commitment, real-time unit commitment, and real-time economic dispatch cycles. To evaluate the revenue gained from supplying heating loads, a flat-rate of \$32.38/MW_t from a regulated Swedish district heating market[42] is adopted. It is observed that the proposed N-R HES operation framework always results in a higher revenue, due to the increased benefits from the reserve market. The revenue earned from energy market remains similar. In addition, there is a significant revenue increase from district heating supply during cold days as shown in Table IV. It is seen that the proposed IREM strategy reaps more benefit for the N-R HES in days with abundant renewables than that in days with scarce renewables, where the revenue growth ranges from 1.55% to 35.25% at different cases. The proposed approach also reduces the total cost of the NREL-118 bus system operation, which is shown in Table V. The

TABLE III. Temperature profile in DHN (J represents junction).

Temperature	J-1	J-2	J-3	J-4
Nominal setpoint (K)	378.15	343.15	338.15	315.15
Pipe-flow result (K)	378	343	338	315
Deviation (%)	0.039	0.043	0.044	0.047

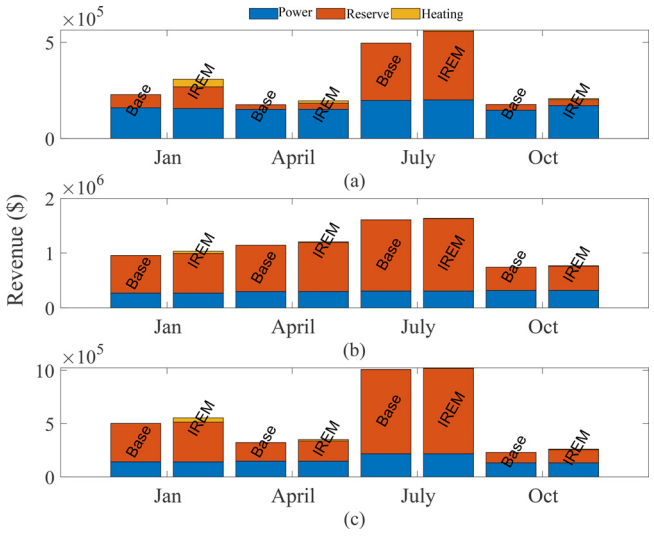

FIG. 19. Comparison of economic benefits for N-R HES between the baseline and the proposed IREM strategy in (a) DASCUC, (b) RTSCUC, and (c) RTSCED.

TABLE IV. Numerical comparison of the total revenue between the proposed IREM strategy and the baseline in DASCUC, RTSCUC, and RTSCED results.

	DASCUC			RTSCUC			RTSCED		
Day	Baseline ($)	IREM ($)	Δ(%)	Baseline ($)	IREM ($)	Δ(%)	Baseline ($)	IREM ($)	Δ(%)
January 1	227 980	308 360	35.25	954 910	1 032 075	8.08	502 300	554 450	10.38
April 1	175 800	196 110	11.55	1 142 510	1 205 430	5.51	322 700	350 860	8.72
July 1	495 600	563 518	13.70	1 608 090	1 635 538	1.70	1 008 300	1 024 018	1.55
October 1	176 780	207 743	17.51	738 530	766 863	3.83	229 600	261 643	13.95

TABLE V. Comparison of the total operation cost of the NREL-118 bus system between the cases with and without IREM strategy.

Day	Total cost		
	Without IREM ($)	With IREM ($)	Δ($)
January 1	2.4504×10^8	2.4480×10^8	-2.4×10^5
April 1	2.6217×10^8	2.6150×10^8	-6.6907×10^5
July 1	3.6157×10^8	3.6149×10^8	-8.0×10^4
October 1	2.2589×10^8	2.2578×10^8	-1.1×10^5

TABLE VI. Comparison of the reliability metric CPS2 between the cases with and without the IREM strategy.

Day	CPS2		
	Without IREM (%)	With IREM (%)	Δ(%)
January 1	99.31	99.31	···
April 1	99.31	99.61	+0.30
July 1	95.14	95.14	···
October 1	98.61	99.41	+0.80

reduction in cost varies based on the system condition. For example, when the demand is comparatively higher (e.g., July), the system has a lack of capacity to deploy for ancillary services.

To evaluate the reliability benefits of the proposed IREM approach, the AGC model simulation results were leveraged to calculate the Control Performance Standard 2 (CPS2) metric presented in Table VI. The inclusion of N-R HES to the system has slightly improved the CPS2 value in the days of April and October, whereas it remains the same in January and July. The same CPS2 values indicate the possible depletion of available resources to meet the system demand while no surplus to improve the reliability further.

V. CONCLUSION

In this paper, a multi-timescale electricity market simulation model was developed and customized to maximize the benefits of grid-connected N-R HES from the perspective of energy and reserve export. A three-cycle model was considered, including two hourly and sub-hourly unit commitment models and one real-time dispatch model. The N-R HES was employed in a price-maker role rather than in the conventional price-taker role. A DHN was integrated into the detailed NREL-118 test system as a lumped thermal load. The thermal dispatch values for DHN were verified in a detailed pandapipes DHN model (a hydraulic-thermal model). The proposed approach resulted in higher revenue than the regular grid connected N-R HES in all the considered cases. Potential future work will explore methods for the asynchronous coordination between electricity and thermal products with a more detailed SMR model.

ACKNOWLEDGMENTS

This material is based upon work supported by the U.S. Department of Energy under Award No. DE-NE0008899.

AUTHOR DECLARATIONS

Conflict of Interest

The authors have no conflicts to disclose.

Author Contributions

Jubeyer Rahman: Conceptualization (equal); Data curation (equal); Formal analysis (equal); Investigation (equal); Methodology (equal); Validation (equal); Visualization (equal); Writing – original draft (equal). **Jie Zhang:** Conceptualization (equal); Funding acquisition (equal); Investigation (equal); Methodology (equal); Project administration (equal); Supervision (equal); Writing – review & editing (equal).

DATA AVAILABILITY

The data that support the findings of this study are available from the corresponding author upon reasonable request.

REFERENCES

[1]E. Lannoye, D. Flynn, and M. O'Malley, "Evaluation of power system flexibility," IEEE Trans. Power Syst. **27**, 922–931 (2012).
[2]M. Cui, J. Zhang, H. Wu, and B.-M. Hodge, "Wind-friendly flexible ramping product design in multi-timescale power system operations," IEEE Trans. Sustainable Energy **8**, 1064–1075 (2017).
[3]B. Li and J. Zhang, "A review on the integration of probabilistic solar forecasting in power systems," Sol. Energy **210**, 68–86 (2020).
[4]O. M. Babatunde, J. L. Munda, and Y. Hamam, "Power system flexibility: A review," Energy Rep. **6**, 101–106 (2020).
[5]L. Michi, G. Donnini, C. Giordano, F. Scavo, E. Luciano, B. Aluisio, C. Vergine, M. Pompili, S. Lauria, L. Calcara *et al.*, "New HVDC technology in pan-European power system planning," in *AEIT HVDC International Conference (AEIT HVDC)* (IEEE, 2019), pp. 1–6.

[6]A. Gravelsins, G. Bazbauers, A. Blumberga, and D. Blumberga, "Power sector flexibility through power-to-heat and power-to-gas application—System dynamics approach," Environ. Clim. Technol. **23**, 319–332 (2019).
[7]H. Guo, C. Zheng, H. H.-C. Iu, and T. Fernando, "A critical review of cascading failure analysis and modeling of power system," Renewable Sustainable Energy Rev. **80**, 9–22 (2017).
[8]N. I. Voropai, V. A. Stennikov, and E. A. Barakhtenko, "Integrated energy systems: Challenges, trends, philosophy," Stud. Russ. Econ. Dev. **28**, 492–499 (2017).
[9]M. F. Ruth, O. R. Zinaman, M. Antkowiak, R. D. Boardman, R. S. Cherry, and M. D. Bazilian, "Nuclear-renewable hybrid energy systems: Opportunities, interconnections, and needs," Energy Convers. Manage. **78**, 684–694 (2014).
[10]O. K. Bishoge, G. G. Kombe, and B. N. Mvile, "Renewable energy for sustainable development in sub-Saharan African countries: Challenges and way forward," J. Renewable Sustainable Energy **12**, 052702 (2020).
[11]P. R. Shukla, S. Dhar, and J. Fujino, "Renewable energy and low carbon economy transition in India," J. Renewable Sustainable Energy **2**, 031005 (2010).
[12]A. Aslani, E. Antila, and K.-F. V. Wong, "Comparative analysis of energy security in the Nordic countries: The role of renewable energy resources in diversification," J. Renewable Sustainable Energy **4**, 062701 (2012).
[13]E. Guelpa, L. Marincioni, S. Deputato, M. Capone, S. Amelio, E. Pochettino, and V. Verda, "Demand side management in district heating networks: A real application," Energy **182**, 433–442 (2019).
[14]J. Cox, C. Murphy, and A. Foss, "Principles to adapt financing mechanisms for fully integrated hybrid energy systems," J. Renewable Sustainable Energy **14**, 052301 (2022).
[15]J. Rahman and J. Zhang, "Optimization of nuclear-renewable hybrid energy system operation in forward electricity market," in *IEEE Green Technologies Conference (GreenTech)* (IEEE, 2021), pp. 462–468.
[16]M. Cui, J. Zhang, B.-M. Hodge, S. Lu, and H. F. Hamann, "A methodology for quantifying reliability benefits from improved solar power forecasting in multi-timescale power system operations," IEEE Trans. Smart Grid **9**, 6897–6908 (2017).
[17]C. A. McMillan, R. Boardman, M. McKellar, P. Sabharwall, M. Ruth, and S. Bragg-Sitton, "Generation and use of thermal energy in the U.S. industrial sector and opportunities to reduce its carbon emissions," Technical Report No. NREL/TP-6A50-66763 [National Renewable Energy Laboratory (NREL), Golden, CO, 2016].
[18]Y. Xu, Z. Wang, W. Sun, S. Chen, Y. Wu, and B. Zhao, "Unit commitment model considering nuclear power plant load following," in *International Conference on Advanced Power System Automation and Protection* (IEEE, 2011), Vol. 3, pp. 1828–1832.
[19]H. E. Garcia, J. Chen, J. S. Kim, M. G. McKellar, W. R. Deason, R. B. Vilim, S. M. Bragg-Sitton, and R. D. Boardman, "Nuclear hybrid energy systems regional studies: West Texas & Northeastern Arizona," Technical Report No. INL/EXT-15-34503 [Idaho National Laboratory (INL), Idaho Falls, ID, 2015].
[20]B. E. Türkay and A. Y. Telli, "Economic analysis of standalone and grid connected hybrid energy systems," Renewable Energy **36**, 1931–1943 (2011).
[21]J. Chen and H. E. Garcia, "Economic optimization of operations for hybrid energy systems under variable markets," Appl. Energy **177**, 11–24 (2016).
[22]B. Poudel and R. Gokaraju, "Optimal operation of SMR-RES hybrid energy system for electricity & district heating," IEEE Trans. Energy Convers. **36**, 3146–3155 (2021).
[23]Y. Chen, W. Wei, F. Liu, E. E. Sauma, and S. Mei, "Energy trading and market equilibrium in integrated heat-power distribution systems," IEEE Trans. Smart Grid **10**, 4080–4094 (2018).
[24]J. Wang, Z. Wei, B. Yang, Y. Yong, M. Xue, G. Sun, H. Zang, and S. Chen, "Two-stage integrated electricity and heat market clearing with energy stations," IEEE Access **7**, 44928–44938 (2019).
[25]Y. Li, F. Bu, J. Gao, and G. Li, "Optimal dispatch of low-carbon integrated energy system considering nuclear heating and carbon trading," J. Cleaner Prod. **378**, 134540 (2022).
[26]A. A. Al Kindi, M. Aunedi, A. M. Pantaleo, G. Strbac, and C. N. Markides, "Thermo-economic assessment of flexible nuclear power plants in future low-carbon electricity systems: Role of thermal energy storage," Energy Convers. Manage. **258**, 115484 (2022).
[27]B. Poudel and R. Gokaraju, "Small modular reactor (SMR) based hybrid energy system for electricity & district heating," IEEE Trans. Energy Convers. **36**, 2794–2802 (2021).
[28]E. Ela, B. Palmintier, I. Krad, and USDOE Office of Electricity Delivery and Energy Reliability, FESTIV (Flexible Energy Scheduling Tool for Integrating Variable generation), computer software, USDOE Office of Electricity, 2019, https://www.osti.gov//servlets/purl/1504740; https://doi.org/10.11578/dc.20190403.2.
[29]I. Peña, C. B. Martinez-Anido, and B.-M. Hodge, "An extended IEEE 118-bus test system with high renewable penetration," IEEE Trans. Power Syst. **33**, 281–289 (2017).
[30]WN Association, see https://www.world-nuclear.org/information-library/nuclear-fuel-cycle/nuclear-power-reactors/small-nuclear-power-reactors for "Small Nuclear Power Reactors" (accessed December 1, 2022).
[31]TAMU, see https://electricgrids.engr.tamu.edu/electric-grid-test-cases/activsg2000/ for "Electric Grid Test Case Repository" (accessed November 10, 2020).
[32]A. Lokhov, "Load-following with nuclear power plants," NEA News **29**, 18–20 (2011), https://www.oecd-nea.org/nea-news/2011/29-2/nea-news-29-2-load-following-e.pdf.
[33]S. Kasahara, T. Murata, Y. Kamiji, A. Terada, X. Yan, Y. Inagaki, and M. Mori, "Heat transport analysis in a district heating system applying waste heat from GTHTR300, a commercial design of high-temperature gas-cooled reactor," Mech. Eng. J. **3**, 15–00616 (2016).
[34]X. Yan, H. Noguchi, H. Sato, Y. Tachibana, K. Kunitomi, and R. Hino, "Study of an incrementally loaded multistage flash desalination system for optimum use of sensible waste heat from nuclear power plant," Int. J. Energy Res. **37**, 1811–1820 (2013).
[35]H. Safa, "Heat recovery from nuclear power plants," Int. J. Electr. Power Energy Syst. **42**, 553–559 (2012).
[36]D. Lohmeier, D. Cronbach, S. R. Drauz, M. Braun, and T. M. Kneiske, "Pandapipes: An open-source piping grid calculation package for multi-energy grid simulations," Sustainability **12**, 9899 (2020).
[37]H. D. Baehr and K. Stephan, *Heat and Mass Transfer*, 6th ed. [Waerme- und Stoffuebertragung] (Springer, 2008).
[38]A. Schwele, "Integration of electricity, natural gas and heat systems with market-based coordination," Ph.D. thesis (Technical University of Denmark, 2020).
[39]S. Quoilin, see https://github.com/energy-modelling-toolkit/Dispa-SET/tree/master/Database/Heat_demand, for "Dispa-Set" (accessed July 6, 2021].
[40]NREL, http://www.nrel.gov/esif/assets/docs/input-files.zip for "NREL-118 System Database" (accessed November 10, 2020).
[41]See http://docs.oithpc.utdallas.edu/ for "Ganymede-User-Guide" (accessed March 2, 2020).
[42]H. Li, Q. Sun, Q. Zhang, and F. Wallin, "A review of the pricing mechanisms for district heating systems," Renewable Sustainable Energy Rev. **42**, 56–65 (2015).